Ab initio electronic structure calculation of disorder ternary alloys: A reciprocal-space formulation

Aftab Alam
Department of Materials Science and Engineering, University of Illinois, Urbana-Champaign, Illinois 61801, USA

Abhijit Mookerjee
Advanced Materials Research Unit and Department of Materials Science, S.N. Bose National Center for Basic Sciences, JD Block, Sector III, Salt Lake City, Kolkata 700 098, India

(Received 17 November 2009; revised manuscript received 8 April 2010; published 7 May 2010)

Using first-principles density-functional calculations, we present a formalism for a reciprocal-space study of the electronic structure of random ternary alloys. The formalism is based on the augmented-space recursion introduced earlier by us in conjunction with the tight-binding linearized muffin-tin orbital method. Emphasis shall be given to the configurationally averaged Bloch spectral function, which will be a key quantity of our formalism and the reflection of its nature on the density of states will be discussed. We showcase the feasibility of our formalism by applying to two different alloy systems namely: face-centered-cubic based $Cu_{1-x-y}Ni_xZn_y$ alloy and the series of disordered ternary Invar alloys, $Fe_{1-x-y}Ni_xX_y$ $[X=Co,Pd,Pt]$. The effects of short-range ordering and the magnetic properties of these alloys will be discussed in some detail and it will be shown that our predicted magnetic moment agrees well with earlier results.

DOI: 10.1103/PhysRevB.81.184205 PACS number(s): 71.15.Mb, 71.23.−k, 71.20.Be

I. INTRODUCTION

From semiconductor alloys used in devices to brasses and stainless steels, most commercial alloys of practical interest are multicomponent and multiphase systems. There have been extensive studies of the electronic structure of disordered binary alloys. However, studies of disordered ternary and quaternary alloy systems are relatively rare. Although binary alloys provide a first step in the understanding of disordered multicomponent alloy systems, a direct electronic structure calculation of the higher order alloy systems would go a long way to demonstrate the real predictive power of a theory leading to the possibility of alloy design. For a first-principles calculation, in addition to accurate description of the electronic structure part, disordered alloys also demand a reasonable scheme for performing configuration averaging. Over the past three decades, effective-medium theories have proven to be of great use in the study of substitutionally disordered crystals. For homogeneous disorder, configuration-averaged physical quantities are translationally invariant quantities and as such they permit the arsenal of techniques familiar in the analysis of ordered systems like lattice Fourier transforms to be applied without taking recourse to the use of computationally expensive supercells.

One well-known means of determining the effective medium is provided by the coherent-potential approximation (CPA),[1] which represents the state-of-the-art method for describing the configuration-averaged electronic structure of disordered systems.[2,3] The CPA chooses any single site and replaces its environment by a nonrandom, lattice translationally invariant effective medium, which is self-consistently obtained by ensuring that there is no extra scattering on the average due to the configuration fluctuations at that chosen site. The approximation, therefore, cannot properly incorporate effects due to correlated scattering arising out of more than one site. In spite of its success, the CPA, being a single-site approximation, has its own limitation. In particular, it does not work well in the impurity bands for split-band alloys where there is considerable signature of statistical clustering of the impurity atom in the host background. This was investigated by Hüfner *et al.*[4] in the Ni minority bands of Cu-rich NiCu and Pd minority bands of Ag-rich AgPd alloys. As a single-site approximation it is inherently incapable of dealing with short-range-order (SRO) effects. Nor can it describe fluctuations in the crystal potential arising from the disorder in the environment of each site. These statistical fluctuations are responsible for band tailing and sharp clusters-related structure in the density of states (DOS), which in turn yields **k**-dependent momentum-state lifetimes. In addition CPA cannot take into account the effects of off-diagonal disorder arising out of local lattice distortions due to size mismatch of alloying components.

As far as the generalizations of the CPA are concerned, only a few maintain the proper analytic properties and local symmetries of the approximated averaged quantities. Among the successful generalizations we can count the special quasirandom structures proposed by Zunger,[5] the reciprocal-space renormalization based nonlocal CPA (NL-CPA),[6] the traveling-cluster approximation,[7] the itinerant coherent-potential approximation,[8] and the augmented-space recursion (ASR).[9] The last three are based on the augmented-space formalism proposed by one of us.[10] Over the years, the ASR coupled with the tight-binding linearized muffin-tin orbital (TB-LMTO) method[11] has been utilized to provide a systematic way of taking all these important effects into account.[12–14] A more extensive comparison between these different techniques has been given by Tarafder *et al.*[15] and the readers are referred to this paper for an in-depth comparison. We shall show in this paper that the ASR gives a fully *k*-dependent self-energy unlike the CPA. In particular, it should be mentioned that, it has been shown by Rowlands *et al.*[16] that the NL-CPA also yields a fully *k*-dependent self-energy. Short-ranged ordering effects within this technique have been introduced earlier.[17] It is an alternative method in which generalization to ternary alloys will also be interesting. A majority of the applications of the ASR have been

restricted to binary-alloy systems alone. A generalization to ternary alloy systems will be an interesting and useful extension. We ourselves have tentatively begun such a formulation in real space earlier.[18–20] The difficulty and errors that arise in taking a finite real-space cluster for recursion will be overcome in this work by reformulating the theory in reciprocal space. We have to remember, though, that this formulation will hold only if the disorder is homogeneous.

It is the purpose of this paper to present a generalized augmented-space recursion formalism in the reciprocal-space representation for the electronic structure calculation of disordered ternary alloys. Such a formalism will be useful because there are many physical properties which require the configuration average of quantities expressed in terms of reciprocal-space (**k**-space) representations. For example, Bloch spectral functions will be needed if one wants to make a direct comparison with angle-resolved photoemission experimental data or complex band structures, momentum densities, and fuzzy Fermi-surface topology which are probed by Compton scattering and positron-annihilation experiments. Calculation of response functions also require configuration-averaged k-space Green's functions $\langle\langle G(\mathbf{k},z)\rangle\rangle$. The method discussed here is a nontrivial generalization of the earlier technique for binary alloys.[21]

In order to validate our formalism, we have chosen two different class of ternary face-centered-cubic based alloys: $Cu_{1-x-y}Ni_xZn_y$ alloy and a set of Invar magnetic ternary alloys $Fe_{1-x-y}Ni_xX_y$ $[X=Co,Pd,Pt]$.

The first example of alloys also known as *German silver* or *New silver* is of technological interest, which according to the generally accepted interpretation of a large body of experimental investigations[22] undergoes two phase transitions during thermal treatment: (a) at about 774 K from the disordered face-centered-cubic solid solution $Cu_{50}Ni_{25}Zn_{25}$ to an intermediate $L1_2$ phase with local atomic ordering (as deduced from the anomalous x-ray scattering experiments) and (b) at about 600 K to the ordered Heusler-type Cu_2NiZn alloy phase. For completeness and comparison sake we shall discuss the results based on all these three phases.

The second class of ternary alloys $Fe_{1-x-y}Ni_xX_y$ are magnetic Invar systems, which show differing magnetic properties depending on the type of doping element X. The purpose of choosing this set of systems is to make a systematic study of the varying electronic structure properties as a result of different ternary addition from $3d$, $4d$, and $5d$ series to binary Invar $Fe_{65}Ni_{35}$ alloys. In fact we have chosen Co($3d$), Pd($4d$), and Pt($5d$) to be the third component to be added.

The rest of the paper is structured as follows. In Sec. II, we shall describe the augmented-space formalism for the electronic structure of disordered ternary alloys within the framework of TB-LMTO basis. A generalized formulation to study the effects of short-range ordering will be derived in Sec. III. Section IV is devoted for computational details. The results on Bloch spectral function, density of states, and magnetic properties for the two class of alloy systems $Cu_{1-x-y}Ni_xZn_y$ and $Fe_{1-x-y}Ni_xX_y$ $[X=Co,Pd,Pt]$ will be discussed in Sec. V. Concluding remarks will be given in the final section.

II. FORMALISM

Since a central part of our technique require the use of the recursion method,[23] it is essential first to choose a basis in which the Hamiltonian representation is sparse. The TB-LMTO is an ideal basis for the purpose. In the most localized β representation the second-order TB-LMTO Hamiltonian[24] is sparse and can be expressed as

$$\mathbf{H}^{(2)} = \mathbf{H}^{(1)} - \mathbf{h}\ \mathbf{o}\ \mathbf{h}, \tag{1}$$

where

$$\mathbf{H}^{(1)} = \sum_{RL} C_{RL}\mathbf{P}_{RL} + \sum_{RL,R'L'} \Delta_{RL}^{1/2} S_{RL,R'L'} \Delta_{R'L'}^{1/2} \mathbf{T}_{RL,R'L'} \tag{2}$$

and

$$\mathbf{h} = \mathbf{H}^{(1)} - \sum_{RL} E_{\nu RL}\mathbf{P}_{RL},$$

$$\mathbf{o} = \sum_{RL} o_{RL}\mathbf{P}_{RL}. \tag{3}$$

Here R and R' label the unit cells (atomic spheres) on the underlying lattice. $L=(\ell m m_s)$ is the composite angular momentum index. The quantities X_{RL}, where $X=C$, $\Delta^{1/2}$, E_ν, and o are the potential parameters which describe the scattering properties of the atomic potentials at R. For multicomponent alloys, the potential parameters can take on values depending on what kind of atom occupies a particular lattice site. S is the structure matrix which characterizes the full lattice geometry. **P** and **T** are the projection and transfer operators in the Hilbert space spanned by the TB-LMTO basis $\{|RL\rangle\}$. Since augmented-space formalism for disordered alloys has been described in many earlier papers,[25] we shall introduce here only those salient points which will be of direct relevance to our generalization to ternary alloys in **k** space.

A substitutional disordered alloy can be described by a set of discrete random occupation variables $\{n_R\}$ associated with each lattice site R. Any physical observable is a function $f(\{n_R\})$ of these random variables. These random variables n_R for a ternary alloy can take the values 1, 0, and -1 depending on whether the site labeled by R is occupied by an A, B, or C type of atoms. For homogeneous, uncorrelated disorder the probabilities for taking these values are proportional to their concentrations: x_A, x_B, and x_C. We can decompose the joint probability distribution of these variables as $P(\{n_R\}) = \Pi p_R(n_R)$. For ternary alloys each occupation variable n_R can have three possible states, which span a configuration space ϕ_R. The configuration space of the whole set of variables is then $\Phi=\Pi_R^{\otimes}\phi_R$. Formally this configuration space is isomorphic to the configuration space of a lattice of spin 1 objects.

The augmented-space theorem,[25] taking cue from measurement theory, now associates with each random variable n_R a self-adjoint operator $N^R \in \phi_R$, such that its eigenvalues are the values randomly taken by n_R and its projected spectral density is the probability density of that variable,

$$p(n_R) = -\frac{1}{\pi}\lim_{\delta\to 0}\Im m\langle \nu_0^R|[(n_R + i\delta)I - N_R]^{-1}|\nu_0^R\rangle, \quad (4)$$

where $|\nu_0^R\rangle = \sqrt{x_A}|1\rangle + \sqrt{x_B}|0\rangle + \sqrt{x_C}|\bar{1}\rangle$

We can find a representation of N_R as follows:

$$p(n_R) = x_A\delta(n_R - 1) + x_B\delta(n_R) + x_C\delta(n_R + 1) = -\frac{1}{\pi}\lim_{\delta\to 0}\Im m\left\{\frac{x_A}{n_R^+ - 1} + \frac{x_B}{n_R^+} + \frac{x_C}{n_R^+ + 1}\right\},$$

$$n_R^+ = n_R + i\delta. \quad (5)$$

The augmented-space method also tells us, given the probability density, how to find a suitable representation of N^R. The first step is to find a convergent continued fraction expansion $p(N_R)$,

$$p(n_R) = -\frac{1}{\pi}\lim_{\delta\to 0}\Im m\frac{1}{n_R^+ - \alpha_1 - \dfrac{\beta_1^2}{n_R^+ - \alpha_2 - \dfrac{\beta_2^2}{n_R^+ - \alpha_3}}},$$

where the coefficients are

$$\alpha_1 = (x_A - x_C), \quad \beta_0^2 = 0,$$

$$\alpha_2 = N_1^2[(x_A - x_C)(x_B^2 - 4x_Ax_C)], \quad \beta_1^2 = \frac{1}{N_1^2},$$

$$\alpha_3 = -N_1^2x_B(x_A - x_C),$$

$$\beta_2^2 = x_B + N_1^2x_B(x_A - x_C)^2[1 - N_1^2x_B], \quad (6)$$

where

$$\frac{1}{N_1^2} = (x_A + x_C) - (x_A - x_C)^2.$$

The corresponding representation of the self-adjoint operator N^R is a 3×3 matrix,

$$N_{ij}^R = \begin{pmatrix} \alpha_1 & \beta_1 & 0 \\ \beta_1 & \alpha_2 & \beta_2 \\ 0 & \beta_2 & \alpha_3 \end{pmatrix} \quad (7)$$

and the operator is

$$N_R = \alpha_1\mathcal{P}_R^0 + \alpha_2\mathcal{P}_R^1 + \alpha_3\mathcal{P}_R^2 + \beta_1\mathcal{T}_R^{01} + \beta_2\mathcal{T}_R^{12}. \quad (8)$$

The eigenvalues of this matrix are -1, 0, and 1 and the corresponding eigenkets are $|\bar{1}\rangle$, $|0\rangle$, and $|1\rangle$. The basis in which this tridiagonal representation is expressed is $|\nu_0^R\rangle$, $|\nu_1^R\rangle$, and $|\nu_2^R\rangle$. The last two are the two mutually orthogonal kets to $|\nu_0^R\rangle$ defined as

$$|\nu_1^R\rangle = N_1[\sqrt{x_A}(1 - x_A + x_C)|1\rangle - \sqrt{x_B}(x_A - x_C)|0\rangle - \sqrt{x_C}(1 + x_A - x_C)|\bar{1}\rangle],$$

$$= h_1|1\rangle + h_2|0\rangle + h_3|\bar{1}\rangle,$$

and

$$|\nu_2^R\rangle = N_2[\sqrt{x_A}\{1 + a - (x_A - x_C)x_BN_1^2\}|1\rangle + a\sqrt{x_B}|0\rangle + \sqrt{x_C}\{1 + a + (x_A - x_C)x_BN_1^2\}|\bar{1}\rangle],$$

$$= g_1|1\rangle + g_2|0\rangle + g_3|\bar{1}\rangle,$$

with

$$a = (x_A - x_C)^2(x_BN_1^2 - 1) - \frac{1}{N_1^2},$$

$$\frac{1}{N_2^2} = x_B[(x_A + x_C) - (x_A - x_C)^2x_BN_1^2].$$

We should note that unlike the corresponding operator for binary randomness, N^R is not idempotent, i.e., $(N^R)^2 = M^R \neq N^R$,

$$M_{ij}^R = \begin{pmatrix} U_1 & V_{12} & V_{13} \\ V_{12} & U_2 & V_{23} \\ V_{13} & V_{23} & U_3 \end{pmatrix} \quad (9)$$

with

$$U_1 = \alpha_1^2 + \beta_1^2, \quad U_2 = \alpha_2^2 + \beta_1^2 + \beta_2^2,$$

$$U_3 = \alpha_3^2 + \beta_2^2, \quad V_{12} = (\alpha_1 + \alpha_2)\beta_1,$$

$$V_{13} = \beta_1\beta_2, \quad V_{23} = (\alpha_3 + \alpha_2)\beta_2. \quad (10)$$

The augmented-space theorem[25] states that the configuration average of a function $f(\{n_R, n_R^2\})$ is a matrix element of the operator $\tilde{f}(\{\tilde{N}_R, \tilde{M}_R\})$ in configuration space Φ obtained by replacing each random variable in $f(\{n_R, n_R^2\})$ by its corresponding operators $\{\tilde{N}_R, \tilde{M}_R\}$. The matrix element is taken between the *reference states*,

$$\langle\langle f(\{n_R, n_R^2\})\rangle\rangle = \langle \nu_0|\tilde{f}(\{\tilde{N}_R, \tilde{M}_R\})|\nu_0\rangle,$$

$$\tilde{N}_R = N_R \otimes I \otimes I \cdots. \quad (11)$$

Each site has three possible configurations states labeled by ν_0, ν_1, and ν_2. The sequence of sites $\{C_1\}$ and $\{C_2\}$ having the configuration states ν_1 and ν_2, respectively, is called the *cardinality sequence*. This cardinality sequence uniquely and completely describes a configuration state of the whole system. Thus a general configuration state is labeled by its cardinality sequence,

$$|\{C_1\},\{C_2\}\rangle = \prod_{\{R_i\in C_1\}}^{\otimes}|\nu_1^{R_i}\rangle \otimes \prod_{\{R_j\in C_2\}}^{\otimes}|\nu_2^{R_j}\rangle \otimes \prod_{R\neq\{C_1\}\cup\{C_2\}}|\nu_0^R\rangle.$$

The *null sequence* $\{\emptyset\}\{\emptyset\}$ is a state all of whose sites are in

a configuration state ν_0. The reference state $|\nu_0\rangle \equiv \Pi_R^{\otimes} |\{\nu_0^R\}$ is labeled by the null sequence since none of its sites have configuration states ν_1 or ν_2 Thus the configuration states $|\{C_1\},\{C_2\}\rangle$ span the full configuration space $\Phi = \Pi_R^{\otimes} \phi_R$.

Any random local potential parameter X_R can now be expressed in terms of n_R as

$$X_R = \frac{1}{2} n_R (1+n_R) X_A + (1-n_R)(1+n_R) X_B + \frac{1}{2} n_R (n_R - 1) X_C, \tag{12}$$

where X_A, X_B, and X_C are the values taken by X_R corresponding to the random variable n_R having the value 1, 0, and −1, respectively. According to augmented-space theorem, the operator representation $\tilde{X}_R$ of X_R is obtained by replacing all n_R by the corresponding operator N^R and all n_R^2 by M^R giving the following expression:

$$\tilde{X}_R = \frac{1}{2}(N^R + M^R) X_A + (\tilde{I} - M^R) X_B + \frac{1}{2}(M^R - N^R) X_C = X_1 \mathbf{I} + X_2 \mathbf{P}_R^0 + X_3 \mathbf{P}_R^1 + X_4 \mathbf{P}_R^2 + X_5 \mathbf{T}_R^{01} + X_6 \mathbf{T}_R^{12} + X_7 \mathbf{T}_R^{02}, \tag{13}$$

where

$$X_1 = X_B,$$

$$X_2 = \frac{1}{2}[\alpha_1 (X_A - X_C) + (X_A - 2X_B + X_C) U_1],$$

$$X_3 = \frac{1}{2}[\alpha_2 (X_A - X_C) + (X_A - 2X_B + X_C) U_2],$$

$$X_4 = \frac{1}{2}[\alpha_3 (X_A - X_C) + (X_A - 2X_B + X_C) U_3],$$

$$X_5 = \frac{1}{2}[\beta_1 (X_A - X_C) + (X_A - 2X_B + X_C) V_{12}],$$

$$X_6 = \frac{1}{2}[(X_A - 2X_B + X_C) V_{13}],$$

$$X_7 = \frac{1}{2}[\beta_2 (X_A - X_C) + (X_A - 2X_B + X_C) V_{23}].$$

The configuration-space operators in the above equations are $\mathbf{P}_R^{\lambda} = |\nu_\lambda^R\rangle\langle\nu_\lambda^R|$, $\lambda = 0,1,2$, and $\mathbf{T}_R^{\lambda\lambda'} = |\nu_\lambda^R\rangle\langle\nu_{\lambda'}^R| + |\nu_{\lambda'}^R\rangle\langle\nu_\lambda^R|$ $\lambda, \lambda' = 0,1,2$.

Equation (13) gives us a prescription of how to set up the augmented-space operators corresponding to the random local potential parameters $\tilde{E}_{\nu RL}$, $\tilde{C}_{RL}$, $\tilde{\Delta}_{RL}^{1/2}$, and $\tilde{\sigma}_{RL}$. The second-order Hamiltonian given by Eq. (1) for a disordered alloy looks like

$$\hat{\mathbf{H}}^{(2)} = \hat{\mathbf{H}}^{(1)} - \hat{\mathbf{h}}\ \hat{\mathbf{o}}\ \hat{\mathbf{h}} \tag{14}$$

with

$$\hat{\mathbf{H}}^{(1)} = \sum_R \underline{\underline{\tilde{C}}}_R \otimes \mathbf{P}_R + \sum_{R,R'} \underline{\underline{\tilde{\Delta}}}_R^{1/2} \underline{\underline{\mathbf{S}}}_{R,R'} \underline{\underline{\tilde{\Delta}}}_{R'}^{1/2} \otimes \mathbf{T}_{RR'},$$

$$\hat{\mathbf{h}} = \tilde{\mathbf{H}}^{(1)} - \sum_R \underline{\underline{\tilde{E}}}_{\nu R} \otimes \mathbf{P}_R,$$

$$\hat{\mathbf{o}} = \sum_R \underline{\underline{\tilde{\sigma}}}_R \otimes \mathbf{P}_R, \tag{15}$$

where the matrix operators are matrices in angular momentum space labeled by L, which is the composite index (lmm_s). $\tilde{C}_{RL}$, $\tilde{E}_{\nu RL}$, $\tilde{\sigma}_{RL}$, and $\tilde{\Delta}_{RL}^{1/2}$ are operators in configuration space of n_R and have the same form as $\tilde{X}_R$ described above. The Hamiltonian is a function of a whole set of random variables $\{n_R, n_R^2\}$, one pair for each site. After replacing all the random variables by their corresponding operator representations, $\hat{\mathbf{H}}^{(2)}$, $\hat{\mathbf{H}}^{(1)}$, $\hat{\mathbf{h}}$, and $\hat{\mathbf{o}}$ are now the operators in an enlarged Hilbert space called the augmented space which is a direct product of the real space (spanned by the TB-LMTO basis) and the configuration space, i.e., $\Psi = \mathcal{H} \otimes \Phi$. Usually the structure matrix $S_{RL,R'L'}$ is not random.

When disorder is homogeneous, the augmented-space Hamiltonian is lattice translationally symmetric. We can jthen define a configuration-averaged Green's function in reciprocal-space representation. This can now be expressed within the augmented-space formalism as

$$\langle\langle G(\mathbf{k},z)\rangle\rangle = \langle \mathbf{k}, L \otimes \{\emptyset\}\{\emptyset\} | (z\tilde{\mathbf{I}} - \tilde{\mathbf{H}}^{(2)})^{-1} | \mathbf{k}, L \otimes \{\emptyset\}\{\emptyset\}\rangle,$$

where $z = E + i\delta$ $(\delta \to 0^+)$.

In general a basis in the $\mathbf{k}$ space has the following form:

$$|\mathbf{k}, L \otimes \{C_1\}\{C_2\}\rangle = \frac{1}{\sqrt{N}} \sum_R e^{-i\mathbf{k}\cdot\mathbf{R}} |R, L \otimes \{C_1\}\{C_2\}\rangle, \tag{16}$$

where $\{C_1\}\{C_2\}$ is the cardinality sequence. One can write this in short-hand notation as $||\{C_1\}\{C_2\}\rangle$, where $||$ stands for $(1/\sqrt{N})\Sigma_R e^{-i\mathbf{k}\cdot\mathbf{R}} |R, L\otimes$. The Bloch spectral function is then defined as

$$A(\mathbf{k},E) = -\frac{1}{\pi} \lim_{\delta\to 0} \Im m[G(\mathbf{k}, E + i\delta)] = -\frac{1}{\pi} \lim_{\delta\to 0} \Im m \langle\{\emptyset\}\{\emptyset\}|| ((E+i\delta)\hat{\mathbf{I}} - \hat{\mathbf{H}}^{(2)})^{-1} ||\{\emptyset\}\{\emptyset\}\rangle. \tag{17}$$

The density of states is then obtained by integrating the Bloch spectral function over the Brillouin zone (BZ),

$$n(E) = \frac{1}{\Omega_{\mathrm{BZ}}} \int_{\Omega_{\mathrm{BZ}}} d\mathbf{k} A(\mathbf{k}, E).$$

We may now combine the above with the recursion method of Haydock *et al.*[23] To do this we need to know how the transfer operators in the augmented Hamiltonian acts on an augmented-space basis. This is shown in the Appendix. Carrying out recursion we obtain the configuration-averaged Green's function as a continued fraction using a similar technique as implemented before[9] for real-space based formalism,

$$\langle\langle G(\mathbf{k},z)\rangle\rangle = \langle\{\emptyset\}||(z\hat{\mathcal{I}} - \hat{\mathbf{H}}^{(2)})^{-1}||\{\emptyset\}\rangle$$

$$= \cfrac{1}{z - a_1 - \cfrac{b_1^2}{z - a_2 - \cfrac{b_2^2}{\ddots z - a_N - T(z)}}}.$$

This can also be written in the form $1/[E-E_0(\mathbf{k})-\Sigma(E,\mathbf{k})]$ [for $z\rightarrow(E+i0^+)$]. It can be easily shown that $a_1=E_0(\mathbf{k})$, the energy dispersion in the absence of disorder. The self-energy $\Sigma(E,\mathbf{k})$ may also be read out directly from the continued fraction. The only approximation involved has to do with the termination of this continued fraction. The coefficients (a_n,b_n) are calculated exactly up to a finite number of steps (N) and the asymptotic part is replaced by a terminator $T(z)$. Haydock[23] has shown that if one carry out recursion exactly up to n steps, the resulting continued fraction maintains the first $2n$ moments of the exact result. Several terminators are available in the literature and we have chosen to use that of Beer and Pettifor.[26] Additionally such an approximation maintains the Herglotz analytic properties of the configuration-averaged Green's function.

We carried out tests for the convergence of energy moments of spectral function with the number of recursion steps before terminating the continued fraction, as suggested by Haydock.[27] Our results have been quoted for 12 recursion steps, leading to 24 moments being accurate.

III. SHORT-RANGED ORDER

As mentioned earlier, the ASR can take into account the effects of configuration fluctuations of not only a single site but also its immediate environment. Significant benefits from the use of ASR may be found when SRO effects are included. In this section we shall generalize the ideas of the previous section to include SRO effects in ternary alloys.

When SRO is present the occupation variables $\{n_R\}$ are correlated. Mookerjee and Prasad[28] have proposed a formulation based on the augmented-space technique which takes into account correlated disorder in binary alloys. We shall now propose a generalization to ternary alloys. If we choose any site R_0 and suppose that n_{R_0} is correlated with the neighboring $\{n_{R_k}\}$ $k=1,2,\ldots,p$, then the joint probability distribution of all the variables can be expanded as

$$P(n_{R_0},n_{R_1},\ldots,n_{R_p},n_{R_{p+1}},\ldots)$$

$$= p(n_{R_0})\prod_{k=1}^{p} p(n_{R_k}|n_{R_0},\ldots,n_{R_{k-1}})\prod_{k>p}^{\infty} p(n_{R_k}).$$

Note that if the SRO is itself homogeneous, it is immaterial which site we choose as R_0. The representation of the operator associated with the random variable n_{R_0} corresponding to the probability density $p(n_{R_0})$ is given by Eq. (8).

Let us now come to the variables n_{R_k}, $k=1,2,\ldots,p$ which are correlated with n_{R_0} but not to one another. We now have to deal with the conditional probability densities depending on the value taken by the variable n_{R_0}. For each such value taken by n_{R_0}, we associate the corresponding conditional probability density $p(n_{R_k}|n_{R_0}=j)$, where $j=0$, 1, or 2. Since the conditional probability densities are also positive definite and assumed to have finite moments to all orders, we may associate with them operators $N_{R_k}^{(j)}$ such that

$$p(n_{R_k}|n_{R_0}=j) = \cdots - \frac{1}{\pi}\lim_{\delta\rightarrow 0}\Im m\langle\nu_0^{R_k}|[(n_{R_k}+i\delta)I - N_{R_k}^{(j)}]^{-1}|\nu_0^{R_k}\rangle.$$

The operator we wish to associate with the variable n_{R_k} should be that $N_{R_k}^{(j)}$ which corresponds to the particular configuration j which n_{R_0} takes. A natural generalization then takes the form

$$\tilde{N}_{R_k} = \sum_j P_{R_0}^{(j)} \otimes N_{R_k}^{(j)} \otimes I \otimes I \otimes \cdots\cdots, \tag{18}$$

where $P_{R_0}^{(j)}$ are the projection operators which project onto the eigenstates $|j\rangle$ of N_{R_0}.

The operators associated with all further sites R_{p+1} are the same as Eq. (8), as they are uncorrelated with R_0. The basic augmented-space theorem still holds good rigorously, but $\tilde{N}_{R_k}$, instead of being of the form given by Eq. (11), now has the form given by Eq. (18).

The SRO in ternary alloy is described by three distinct Warren-Cowley parameters α_{AB}, α_{BC}, and α_{AC} which describe pair correlations between occupations of the three distinct pairs of components. If $P_{\gamma\gamma'}$ is the probability of the central site R_0 being occupied by a γ type atom and the site R_k being occupied by an γ' type atom, then by definition

$$P_{AB} = x_B(1-\alpha_{AB}) \quad P_{AC} = x_C(1-\alpha_{AC})$$

$$P_{AA} = 1 - (P_{AB} + P_{AC}) = (x_A + x_B\alpha_{AB} + x_C\alpha_{AC}), \tag{19}$$

where $x_A+x_B+x_C=1$.

The conditional probability densities $p(n_{R_k}|n_{R_0}=j)$ $(j=1,0,-1)$ associated with the sites belonging to the first-nearest-neighbor (NN) shell can be expressed in terms of the Warren-Cowley SRO parameters as

$$p(n_{R_k}|n_{R_0}=j) = X_A^{(j)}\delta(n_{R_k}-1) + X_B^{(j)}\delta(n_{R_k}) + X_C^{(j)}\delta(n_{R_2}+1)$$

where

$$X_A^{(1)} = x_A + (x_B\alpha_{AB} + x_C\alpha_{AC}),$$

$$X_B^{(1)} = x_B(1-\alpha_{AB}), \quad X_C^{(1)} = x_C(1-\alpha_{AC}),$$

$$X_A^{(0)} = x_A(1-\alpha_{AB}),$$

$$X_B^{(0)} = x_B + (x_A\alpha_{AB} + x_C\alpha_{BC}), \quad X_C^{(0)} = x_C(1-\alpha_{BC}),$$

$$X_A^{(\bar{1})} = x_A(1-\alpha_{AC}),$$

$$X_B^{(\bar{1})} = x_B(1-\alpha_{BC}), \quad X_C^{(\bar{1})} = x_C + (x_A\alpha_{AC} + x_B\alpha_{BC}).$$

In absence of SRO, i.e., $\alpha_{AB}=\alpha_{BC}=\alpha_{AC}=0$, the conditional probabilities of second variable n_{R_k} becomes identical to the unrestricted probability density of the variable n_{R_0}.

Since we have chosen to include conditional probabilities which incorporate pairwise correlations alone, these are the only correlation coefficients in the model. Three site correlations would have required further such parameters: $\alpha_{(A,BC)}$, $\alpha_{(B,AC)}$, $\alpha_{(C,AB)}$, and $\alpha_{(ABC)}$. These we have ignored in our present model.

The representation of the conditional operators are

$$N_{R_k}^{(j)} = a_1^{(j)}\mathcal{P}_{R_k}^0 + a_2^{(j)}\mathcal{P}_{R_k}^1 + a_3^{(j)}\mathcal{P}_{R_k}^2 + b_1^{(j)}\mathcal{T}_{R_k}^{01} + b_2^{(j)}\mathcal{T}_{R_k}^{12}, \quad (20)$$

where

$$a_1^{(j)} = (X_A^{(j)} - X_C^{(j)}),$$

$$b_1^{(j)^2} = (X_A^{(j)} + X_C^{(j)}) - (X_A^{(j)} - X_C^{(j)})^2,$$

$$a_2^{(j)} = \frac{a_1^{(j)} X_B^{(j)}}{b_1^{(j)^2}} - a_1^{(j)},$$

$$b_2^{(j)^2} = X_B^{(j)} + a_2^{(j)} a_3^{(j)}; \quad a_3^{(j)} = -a_2^{(j)} - a_1^{(j)}. \quad (21)$$

In Eq. (18) we also require representations of the projection operators $P_{R_0}^{(j)}$. Since all our representations so far were in the basis in which N_{R_0} were tridiagonal, it is in this basis that the representations have to be made. The representations have been derived in detail in a previous paper (Ref. 20) and the readers are referred to that paper for mathematical details. The representations are of the form

$$P_{R_0}^{(1)} = \begin{pmatrix} x_A & \sqrt{x_A x_B} & \sqrt{x_A x_C} \\ \sqrt{x_A x_B} & x_B & \sqrt{x_B x_C} \\ \sqrt{x_A x_C} & \sqrt{x_B x_C} & x_C \end{pmatrix},$$

$$P_{R_0}^{(0)} = \begin{pmatrix} h_1^2 & h_1 h_2 & h_1 h_3 \\ h_1 h_2 & h_2^2 & h_2 h_3 \\ h_1 h_3 & h_2 h_3 & h_3^2 \end{pmatrix},$$

and

$$P_{R_0}^{(\bar{1})} = \begin{pmatrix} g_1^2 & g_1 g_2 & g_1 g_3 \\ g_1 g_2 & g_2^2 & g_2 g_3 \\ g_1 g_3 & g_2 g_3 & g_3^2 \end{pmatrix}. \quad (22)$$

We may now explicitly obtain the expressions for the operators $\tilde{N}_{R_k}$. The explicit expression is given in the Appendix of Ref. 20. It will be useful to examine the expression in that reference in some detail. We note from Eq. (8) that when SRO is absent the augmented-space operator $\tilde{N}_R$ creates, annihilates, or counts configuration fluctuations only at the site R. However, the generalized operator $\tilde{N}_{R_k}$ not only creates, annihilates, or counts configuration fluctuations at the site R_k but also at the correlated site R_0. In addition it also creates, annihilates, or counts configuration fluctuations *simultaneously* at both the sites R_k and R_0. In this sense, SRO introduces two site off-diagonal disorder. Single-site mean-field approaches like the CPA cannot take care of such correlated disorder without further approximations. In such situations it would be profitable to use the ASR.

IV. COMPUTATIONAL DETAILS

Before we go onto the actual realistic calculation, it is important to mention at this point that unlike CPA which yields a **k**-independent self-energy, the ASR method yields a self-energy which does depend on **k** starting from the fourth level of recursion coefficients. This has been shown analytically by us in an earlier communication[21] for a single *s*-band nearest-neighbor model. Another advantage of **k**-space recursion (over the real-space one) is the possibility of working in an enormously reduced space (compared to the Hilbert space required in the real-space recursion method). It can be shown explicitly[21] that the operation of the effective Hamiltonian $\hat{\mathbf{H}}^{(2)}$ can entirely be done in the configuration space and the calculation does not require us to involve the real space $\mathcal{H}$ at all. This is an enormous simplification over the standard augmented-space recursion described earlier.[12] Earlier we had to resort to symmetry reduction in this enormous space in order to make the recursion tractable. Here the rank of only the configuration space is much smaller and we may further reduce it by using the local symmetries of the configuration space, as described in an earlier paper.[29]

The total-energy calculations were done using the TB-LMTO-ASR method for disordered ternary alloys in reciprocal-space representation. For our calculation, "clusters" of sizes 1 200 000 states in the enlarged augmented space were generated by repeatedly applying the augmented Hamiltonian on the starting state $||\nu_0\rangle\rangle$. Ten steps of recursion were carried out attached with a terminator by Beer and Pettifor[26] to construct the configuration-averaged Bloch spectral function. In order to calculate the charge densities and the density of states, a Brillouin zone integration was performed using the generalized tetrahedron method[30] developed by us for disordered systems with 280 **k** points in the irreducible wedge of the BZ. The calculations were scalar relativistic with the inclusion of Darwin and the mass-velocity correction terms. The exchange-correlation functional used is that of von Barth and Hedin.[31] In all the calculations, the lattice relaxation effects were included following the treatment suggested by Kudrnovský *et al.*[32] The idea is to choose the atomic sphere approximated radii of various atoms in the system in such a way that the spheres are charge neutral on average. We have utilized this procedure throughout our calculation to correctly take into account the charge-transfer effect which is one of the most important factors in any electronic structure calculation. Total energy, local and average magnetic moment, and total and atom-projected charge and spin densities are all usual products of the calculations. The equilibrium lattice constant used for the calculation of all the three phases of Cu-Ni-Zn system is $a=6.63$ a.u. However the same for magnetic Invar alloys Fe-Ni-Co, Fe-Ni-Pd, and Fe-Ni-Pt are $a=6.69$ a.u., $a=6.81$ a.u., and $a=6.75$ a.u., respectively. These equilibrium lattice parameters were obtained by minimizing the total DFT energies with respect to the lattice parameters. These structural parameters compare quite well with those of the existing theoretical and experimental findings.[22,33]

As already mentioned in Sec. I, for the alloy Cu_2NiZn, three different structural phases are formed during the ther-

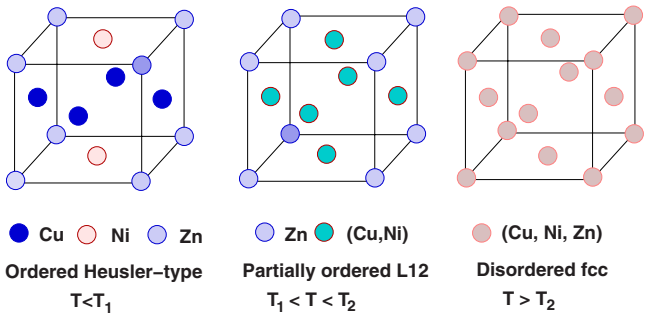

FIG. 1. (Color online) Three possible structural phases of Cu_2NiZn system during thermal processing. The structure in the extreme left is an ordered Heusler type which exists below T_1 =623 K. The middle structure is a partially ordered $L1_2$ type where the cube corners are selectively occupied by Zn atoms however the face centers are substitutionally occupied by Cu and Ni atoms. This phase is also an example of pseudobinary alloys which exists between the temperature range T_1=623 K and T_2=774 K. The structure in the extreme right is the disordered face-centered-cubic solid solution phase where all the sites are randomly occupied by Cu, Ni, and Zn atoms with probabilities 0.5, 0.25, and 0.25, respectively.

mal processing: an ordered Heusler-type Cu_2NiZn alloy phase, an intermediate phase with partial atomic ordering in a $L1_2$-type structure $(Cu_{1-x}Ni_x)_3Zn$, and a completely disordered face-centered-cubic solid solution, $Cu_{1-x-y}Ni_xZn_y$. The structures of these three phases are shown in Fig. 1. For the ordered Cu_2NiZn, the sublattice of cube corner sites [shown by light blue (gray) spheres] is occupied by Zn atoms, the second sublattice of bottom face centers [shown by pink (white) spheres] is occupied by Ni atoms and the remaining sublattice of vertical face centers [shown by dark blue (dark) spheres] is occupied by Cu atoms. In second phase with partial ordering, the cube corners are still occupied by Zn atoms but the remaining sublattices [shown by cyan (dark gray) spheres] are occupied randomly by Cu and Ni atoms with probabilities $\frac{2}{3}$ and $\frac{1}{3}$, respectively. This is a pseudobinary alloy and has been studied by the ASR by us earlier.[34] Finally in the completely disordered face-centered-cubic phase all sites are occupied randomly by Cu, Ni, and Zn atoms with probabilities 0.5, 0.25, and 0.25, respectively. This is shown in the right-most panel in Fig. 1. The two experimental phase-transition temperatures are T_1=623 K and T_2 =774 K. We have also studied the magnetic Invar systems $Fe_{1-x-y}Ni_xX_y$ $[X=Co,Pd,Pt]$ only in the completely disordered face-centered-cubic solid solution phase shown by the extreme right structure in Fig. 1.

The basic philosophy behind the configuration averaging procedure in augmented *real-space* based formalism is to expand the Hilbert space spanned by the TB-LMTO basis (labeled by lattice positions) to include a configuration space which takes into account the statistical fluctuations of the configurations of the system about the "average" configuration. Hence for a system with N sites and m possible realizations of the random variables associated with each site, the augmented space involves Nm^N basis functions. The standard method for implementing this on a computer would require handling an impossibly large $(Nm^N)\times(Nm^N)$ matrices. Working with this large (even though sparse) Hamiltonian becomes a difficult task for realistic alloy systems with *s-p-d* orbitals.

In order to make recursion tractable computationally, we have taken recourse to several techniques which shrink the rank of the Hilbert space on which recursion takes place. Three such techniques have been used by us.

First is recursion in the **k** space itself, which replaces the familiar real-space version. As mentioned before, one requires to deal only with the configuration space (rather than the outer product of real Hilbert space $\mathcal{H}$ and the configuration space Φ). The size of the configuration space is *much* smaller than the full augmented space Ψ. Instead of handling the enormously large matrix of rank $(Nm^N)\times(Nm^N)$ (for a real-space recursion), one need to deal with a matrix of rank $(m^N)\times(m^N)$ only for a **k**-space recursion. In addition, the approximation involved in truncating the full lattice to a large cluster is also avoided.

Second, there are conceptual advantages in the augmented-space formalism. The continued fraction with terminator ensures that the Herglotz analytic properties are automatically preserved. Translational and local lattice symmetries are automatically built into the augmented-space Hamiltonian.

Finally, we have used memory reduction and time saving for augmented-space recursion by the multispin coding technique. One can utilize the bit manipulation techniques and predefined logical functions in the computer to store the basis vectors of configuration space in bits. To make use of the bit manipulation technique for ternary alloys we proceed as follows. We allocate two bits to describe the configuration states of each site. The bit combination (00) or the integer 0 is assigned to the reference state $|\nu_0^R\rangle$, (01) or the integer 1 is assigned to the configuration state $|\nu_1^R\rangle$, and (10) or the integer 2 is assigned to the configuration state $|\nu_2^R\rangle$. The reference state is (00) while the two excitations generated by the Hamiltonian are (01) and (10). In an M-bit machine, each M-bit word can represent up to $(M-1)$ terms as a sequence of 0s and 1s. To store a configuration of a ternary alloy with N lattice points we need $2(N-1)/(M-1)+1$ words, each of which represents an integer (since we need two bits to define the configuration of a given lattice point).

V. RESULTS AND DISCUSSION

A. Cu_2NiZn alloy

Since the Bloch spectral densities in disordered alloys reflect the nature of energy bands in the ordered compounds, we shall first show the band structure of the ordered Heusler-type Cu_2NiZn system along the X-Γ-R line in the simple-cubic Brillouin zone. This is shown in Fig. 2. The parent CuZn is an archetypal split-band system, i.e., the energies of the Cu and Zn *d* bands are very different. However, although CuNi is also a split-band system with much smaller splitting as compared to CuZn, its electronic structure is sufficiently different from that of CuZn. Hence it will be interesting to investigate the characteristics of the ternary alloy when the two parent binary systems are alloyed. The split-band behavior is clearly visible from the band structure specially for Cu and Zn atoms. The narrow flat bands around $\simeq -0.66$ Ry

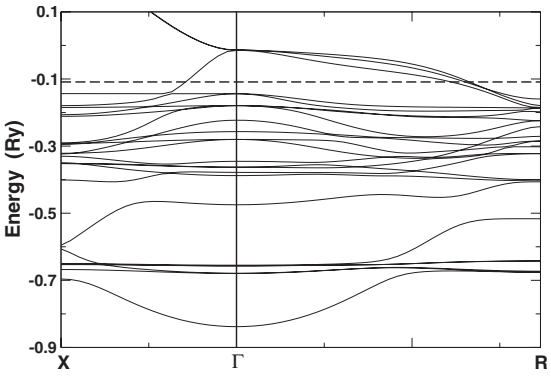

FIG. 2. Band structure of the ordered Heusler-type Cu_2NiZn ($L1_0$ structure) alloy along the line X-Γ-R. Fermi level E_F is indicated by the horizontal dashed line.

reflect the Zn d bands. The Cu d-band complex lies well above the Zn d bands in the energy range $(-0.38, -0.25)$ Ry. The Ni-related d bands are located around $\simeq -0.15$ Ry just above the Cu bands.

We shall now show the Bloch spectral densities for the fully disordered alloys. The spectral density for an ordered compound is given by a bunch of δ-function peaks at energies $E_n(k)$, where n is the band index. In random alloys these peaks are shifted and broadened by disorder. In Fig. 3 we have shown the spectral densities calculated both from our TB-LMTO-ASR and also using Korringa-Kohn-Rostocker (KKR) CPA.[35] We have plotted the Bloch spectral functions for completely disordered $Cu_{50}Ni_{25}Zn_{25}$ alloy along the line X-Γ (lower panel) and Γ-L (upper panel). The various curves in each of the panels indicate the spectral functions at various

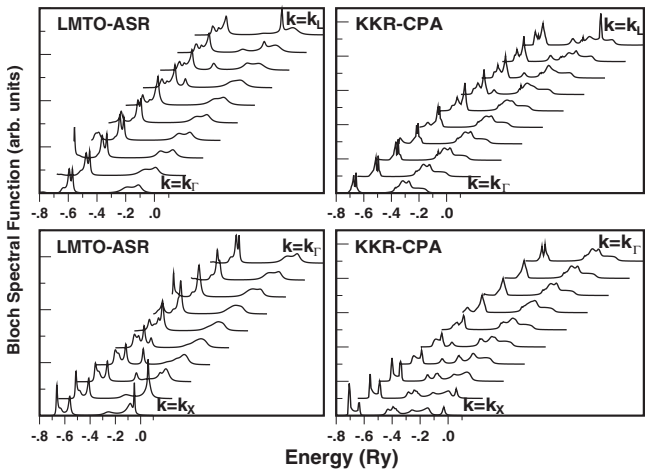

FIG. 3. (Left panels) Bloch spectral densities calculated from TBLMTO-ASR for completely disordered $Cu_{50}Ni_{25}Zn_{25}$ alloy along the line X-Γ-L. The lower panel runs from the symmetry points X to Γ and the upper panel from Γ to L. In each of the two panels, the various curves indicate the spectral functions for various $|\mathbf{k}|$ values starting from the edge $|\mathbf{k_X}|$ to center $|\mathbf{k_\Gamma}|$ (lower panel) and from center $|\mathbf{k_\Gamma}|$ to edge $|\mathbf{k_L}|$ (upper panel) of the Brillouin zone. The y axis is in an arbitrary scale with heights scaled to the maximum height. Different curves for different $|\mathbf{k}|$ values are shifted along the x axis in order to facilitate vision. (Right panels) The same results calculated from KKR-CPA.

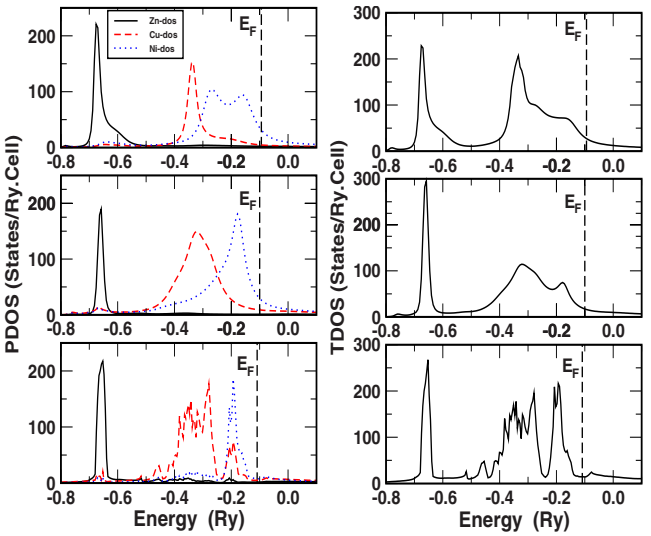

FIG. 4. (Color online) Partial and total density of states for three structural phases of Cu-Ni-Zn system. The lower, bottom, and upper panels on the left show the atom-projected DOS for ordered Heusler-type structure, partially ordered $(Cu_{1-x}Ni_x)_3Zn$ $[x=1/3]$ alloy and completely disordered $Cu_{50}Ni_{25}Zn_{25}$ alloy, respectively. The three panels on the right however show the total DOS for the same three phases. In all the three panels on the left, the solid (black), dashed (red), and dotted (blue) lines indicate the partial DOS for Zn, Cu, and Ni atoms, respectively. The Fermi levels are indicated by dashed vertical lines.

$|\mathbf{k}|$ values starting from the edge $|\mathbf{k_X}|$ to center $|\mathbf{k_\Gamma}|$ [lower panel] and then from center $|\mathbf{k_\Gamma}|$ to the edge $|\mathbf{k_L}|$ [upper panel] of the Brillouin zone. The y axis is in an arbitrary scale. In order to facilitate vision, different curves for different $|\mathbf{k}|$ values are shifted along the x axis.

The first observation is that for homogeneously disordered systems, there is little benefit in going to the ASR from CPA. The main difference is in the k dependence of disorder-induced spectral broadening leading to lifetime effects. This we had seen earlier in binary alloys as well.[36]

The split bands can clearly be observed, with low-energy peaks originating from the Zn sites and the high-energy features corresponding to a combined contribution from Cu and Ni sites. As we go along the X-Γ line the doubly peaked structure in the energy regime $E \in (-0.7, -0.57)$ Ry due to the Zn atom broaden out to a single peaked structure with a weak shoulder on the left. Such a broadening is due to the influence of disorder. On the contrary, the complex of Cu and Ni d bands [structure at the higher energy $E \in (-0.4, -0.05)$ Ry] along the same line are comparatively more strongly influenced by the disorder especially in its upper part slightly below the Fermi level $E_F \simeq -0.1$ Ry. Along the line Γ-L, the Zn d-band structure also gets broadened but in this case it is much more asymmetric as we move toward L. In fact we can see broad featureless bumps which do not move with the $\mathbf{k}$ vector indicating a strong influence of disorder. The structure of the combined contribution of (Cu,Ni) bands are again strongly influenced by disorder as is reflected from the large broadening in this energy regime.

The total and the partial density of states (TDOS and PDOS) for the three structural phases of Cu-Ni-Zn system

are presented in Fig. 4. The three panels in the left show the PDOS for the completely ordered Heusler-type structure (lower panel), partially ordered $(Cu_{1-x}Ni_x)_3Zn$ $[x=1/3]$ alloy (middle panel), and completely disordered $Cu_{50}Ni_{25}Zn_{25}$ alloy (upper panel). The three panels on the right show the TDOS for the same three structures. In all the three panels on the left, the Zn, Cu, and Ni PDOS are shown by solid (black), dashed (red), and dotted (blue) lines, respectively. Fermi levels are indicated by the long-dashed vertical lines. The first thing to notice is the direct reflection of the basic features of band structure in the PDOS of the ordered phase (lower panel). As before, the Cu and Ni PDOS are less widely separated in energy as compared to that between Zn and Cu. We notice that the Zn *d* PDOS, which is well separated from the contributions of Cu and Ni, hardly hybridizes with them. However the Cu and Ni PDOS show sufficient hybridization. More specifically a narrow well-separated Zn *d* PDOS (solid line) can be seen to be centered around $E\sim-0.66$ Ry. Most of the Cu *d* PDOS (dashed line) lie in the energy range $(-0.43,-0.24)$ Ry, however a non-negligible contribution of the same is also found in the energy region of the Ni *d* states, i.e., $(-0.23,-0.12)$ Ry. Similarly, the Ni *d* PDOS contributes non-negligibly in the energy region of the Cu *d* PDOS. These contributions, in both the cases, are mediated indirectly via coupling among the simple-cubic sublattices.

If we now look at the PDOS and TDOS for the partially ordered phase shown in the middle panel of Fig. 4, we notice significant dramatic changes specially in the Cu and Ni character. First of all the PDOS on Ni atoms is significantly broadened in comparison to the ordered alloy case. This broadening is mediated by the disorder on the sublattice (face centers) which is occupied randomly by Cu and Ni in proportion 2:1. This broadening is less pronounced for Cu atoms compared to that of Ni because of the NN pair geometry on the underlying sublattice. Another thing to notice in the middle panel is the disappearance of the pseudogap which separated Cu and Ni subbands in the ordered Cu_2NiZn alloy. Interestingly, the PDOS in the energy region of Cu and Ni states resembles closely that of the completely disordered face-centered-cubic phase of the same composition binary alloy[37] (i.e., $Cu_{67}Ni_{33}$). On the contrary, the local DOS on the Zn atoms on the ordered sublattice (cube corner) is only weakly influenced by randomness via coupling with the disordered sublattices because of the large separation of the Zn energy bands from that of the Cu and Ni *d* bands.

The results for the completely disordered phase $Cu_{50}Ni_{25}Zn_{25}$ are shown in the top panel of Fig. 4. We see an additional smearing of total DOS features in the energy range of Cu and Ni states. In fact the broadening in the local DOS on Ni atom is quite dramatic with a weak shoulder on the higher energy side. The most remarkable effect however is the broadening of the Zn *d* bands, which is of course a consequence of the disorder via coupling with the Cu and Ni atoms. It would be interesting to compare our results with the KKR-CPA results of Althoff *et al.*[38] Comparison is between our DOS and the DOS shown in their Fig. 6. There is close resemblance between the results: with well-separated Zn and Cu *d* peaks and the Ni shoulder at higher energies. This confirms our earlier statement that there is not much benefit in going from the CPA to ASR in homogeneously disordered alloys.

TABLE I. Specific choice of Warren-Cowley parameters for the ternary alloy *ABC* and their interpretation.

α_{AB}	α_{AC}	α_{BC}	Type of correlation
0	0	0	No SRO
0	1	1	*AB* alloyed, *C* segregated
0	0	1	*AB*, *AC* alloyed but pairwise segregated
1	0	1	*AC* alloyed, *B* segregated
0	1	0	*AB*, *BC* alloyed but pairwise segregated
1	1	0	*BC* alloyed, *A* segregated
1	0	0	*AC*, *BC* alloyed but pairwise segregated
1	1	1	*A*,*B*,*C* all segregated

We next carry out calculations in the presence of SRO. Single site mean-field theories are unable to deal with SRO. Here the benefit of going to ASR from CPA will be more evident. We have described SRO in terms of Warren-Cowley parameters defined in Eq. (19). The interpretation of these parameters in some specific cases is described in the Table I. In two earlier papers Althoff *et al.*[38,39] used the KKR-CPA to describe the emergence of SRO in disordered $Cu_{50}Ni_{25}Zn_{25}$ by explicitly obtaining the Warren-Cowley parameters from the joint spectral densities of the homogeneously disordered alloy. The aim here is to use the ASR to obtain the densities of states of the alloy in *presence* of SRO. Here the Warren-Cowley parameters enter the problem as parameters. The SRO parameters are chosen in several extremal cases of alloying and segregation so that the maximum effect of their variation is reflected in the results.

The top panel of Fig. 5 shows the spectral functions at the symmetry points k_X, k_Γ, and k_L for $Cu_{50}Ni_{25}Zn_{25}$ at the SRO parameters listed in Table I. We should first note again the Zn-like bands sit in the range −0.8 to −0.6 Ry, the Cu-like bands around −0.4 to −0.3 Ry, and Ni-like bands around −0.2 Ry. The widths of the spectral-function structures are related to disorder-induced finite lifetimes of Bloch-type states. These widths and the relative weights are sensitively dependent on SRO. The disorder-induced widths are related to the disorder-induced self-energies. As we have seen earlier that SRO introduces off-diagonal disorder with correlated configuration fluctuations at a site and its nearest neighbors. This leads to a strong *k* dependence of the self-energy and hence the widths. The CPA gives *k*-independent self-energies and cannot reproduce these results.

The bottom panel of Fig. 5 shows the densities of states with specific values of the Warren-Cowley parameters listed in Table I. It is clear from the various panels that SRO has considerable effect on the DOSs, particularly on the Cu-Ni part of the DOS. In order to understand the effect of SRO on these DOS structures we choose three of the types of SRO presented in Fig. 5: (a) Cu and Ni alloyed and Zn segregated (0-1-1), (b) Cu and Ni and Cu and Zn alloyed but pairwise segregated (0-0-1), and (c) Cu, Ni, and Zn all segregated (1-1-1). In order to understand the effect of SRO on the DOS structures we present in Fig. 6 ordered calculations showing

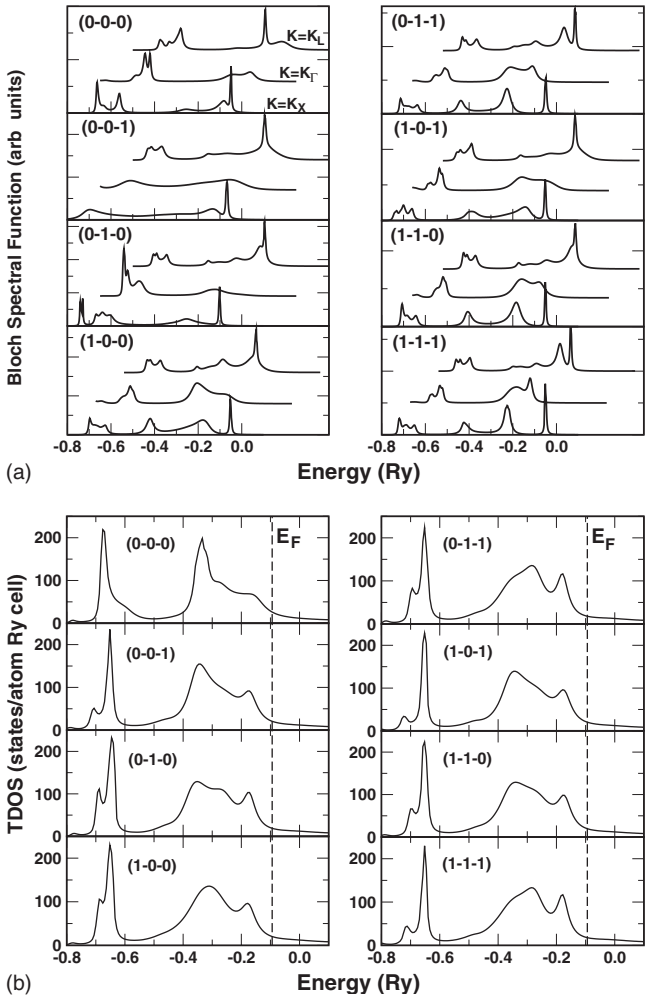

FIG. 5. (Top) Spectral densities at three high-symmetry points k_X, k_Γ, and k_L for various SRO listed in Table I. (Bottom) Densities of states of $Cu_{50}Ni_{25}Zn_{25}$ (top left) without any SRO and (other panels) with SRO parameters.

overlapping DOS of (left) Zn and CuNi, (middle) CuNi and CuZn, and (right) Cu, Ni, and Zn. We first note that the Zn structure is well separated in energy from the Cu and Ni structures. SRO has very little effect on the virtual bound state like structure of Zn. To discuss the Cu-Ni structures we should first remember that when disorder is introduced the resulting self-energy will smoothen the DOS of its fine structure. The cases (0-1-1) and (1-1-1) are rather similar as the CuNi DOS and overlapping Cu and Ni DOS both give rise to two peaks roughly around −0.3 and −0.2 Ry with the former having slightly greater weight as compared to the latter. For the case (0-0-1) the Cu related structures arising from the DOS for CuNi and CuZn do not overlap exactly and introduce a higher weight toward −0.4 Ry. This similarity between the CuNi structures for (0-1-1) and (1-1-1) and difference with (0-0-1) is clearly evident in Fig. 5 bottom panel reinforce each other giving rise to *a*. The CPA would not be able to reproduce these effects.

B. FeNi*X* [*X*=Co,Pd,Pt] alloys

The main motivation behind the application of our formalism in this section is to explore the effects of gradual addition of a third component from 3*d*, 4*d*, and 5*d* series to $Fe_{65}Ni_{35}$ Invar alloy. We have chosen the Co(3*d*), Pd(4*d*), and Pt(5*d*) to be the third component. For all the cases, the concentration of Fe has been fixed to be at 65%. Another reason for choosing these set of alloy systems is to check the predictive power of our formalism for magnetic alloys. All of these alloy systems behave magnetically (nonmagnetically) depending on a range of lattice constant above (below) a critical value. In other words these alloys undergo a phase transition from ferromagnetic to paramagnetic under pressure. The transition can also occur due to the gradual increase in Fe percentage beyond 75%. Our aim in this section however is to explore the electronic structure of these alloy systems within the magnetic regime.

In order to give an idea about the feature of Bloch spectral densities in these classes of magnetic Invar alloy systems, we have chosen $Fe_{65}Ni_{20}Co_{15}$ alloy as a representative candidate the spectral densities for which are shown in Fig. 7. The left panel shows the spectral function for spin up and the right panel for spin down. Other details for both the panels are similar to Fig. 3. The first thing to notice in this figure is the larger broadening of the spectral densities for spin down as compared to that for spin up. In addition, the peak intensities on the higher energy scale are comparatively more Lorenzian broadened. Unlike the Cu-Ni-Zn case, where the individual atom contributions were energetically well separated from each other and hence was easy to identify in terms of band structure (or Bloch spectral functions), the contribution of each individual atoms in FeNiCo case is spread out over the

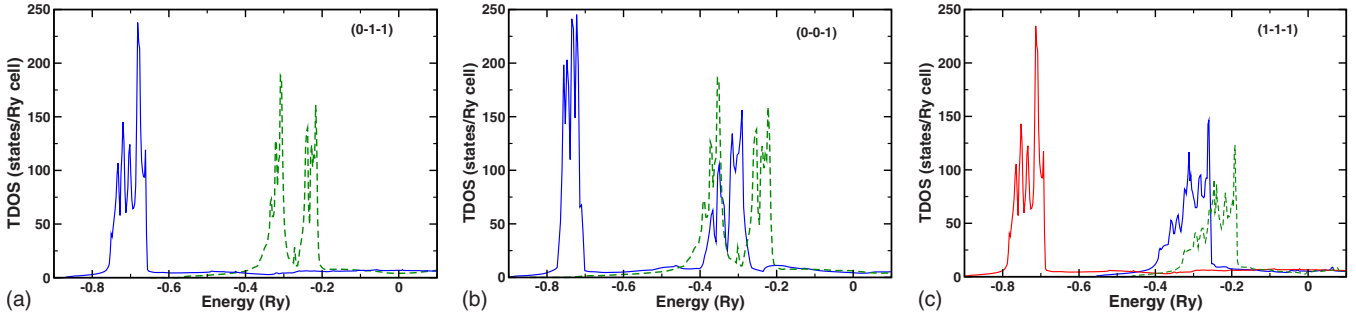

FIG. 6. (Color online) DOS for ordered (left) CuNi and Zn (center) CuNi and CuZn and (right) Cu, Ni, and Zn. This is for comparison and understanding with the possible short-range ordering effects in the Fig. 5.

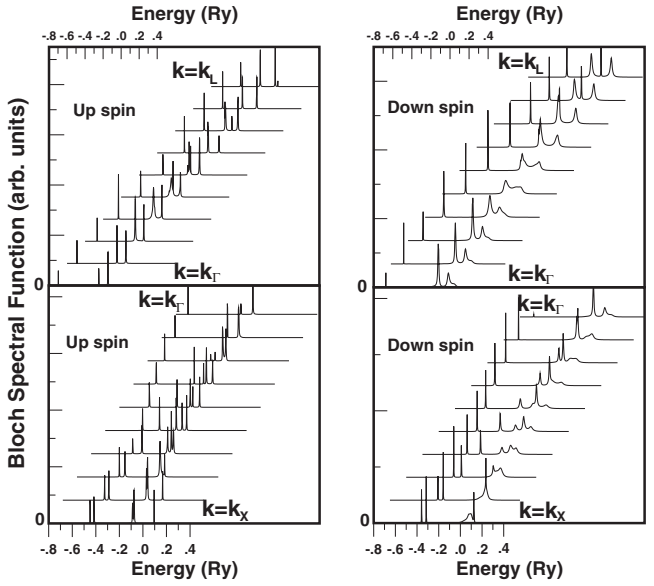

FIG. 7. Bloch spectral densities for fully disordered $Fe_{65}Ni_{20}Co_{15}$ alloy along the line X-Γ-L. The left panel shows the spectral densities for spin up along the symmetry line X to Γ (lower panel) and along Γ to L (upper panel). The right panel on the other hand shows a similar plot but for spin down. Other details are same as Fig. 3.

entire energy range $(-0.6, 0.1)$ Ry. In other words there is a tendency of strong hybridization between the neighboring atoms, which gives rise to mixed character in the Lorenzian shaped spectral densities specially in the higher energy regime $(-0.3, -0.1)$ Ry. In contrast to the spin-up case, it is comparatively easier to locate the individual atom contribution in the spin-down case. This will become more clear if we look at the density of states for $Fe_{65}Ni_{20}Co_{15}$ alloy in the extreme left column of Fig. 8. It is clear from the top left panel of this figure that for spin-down case, the Fe peaks are mostly shifted toward the higher energy range, Ni contribution dies down quickly in the higher energy side however the Co contribution is spread out throughout the energy window. So it is more likely that the higher energy peaks (in Fig. 7) in the spectral density for the spin-down case is coming from a combined contribution of the Fe and Co atoms. There might be a weak contribution from Ni atom due to hybridization. The sharp peaks in the spectral densities at low energy are a combined contribution from all the three constituent atoms.

The upper panel of Fig. 8 shows the component-projected-spin-resolved DOS for disordered $Fe_{65}Ni_{20}Co_{15}$ (left), $Fe_{65}Ni_{20}Pd_{15}$ (middle), and $Fe_{65}Ni_{20}Pt_{15}$ (right) alloys, respectively. The lower panel on the other hand shows the total spin-resolved DOS for the same three alloy systems. One can notice from the upper panel that for Pd and Pt substituted alloys, the peaks related to Pd or Pt are below the Fe and Ni peaks. From the top left panel of Fig. 8, it is clear that the local DOS for majority spins are almost identical for Fe, Ni, and Co while the minority-spin DOS are shifted relative to one another. Among the three constituents, Fe shows the highest exchange splitting between the majority and minority DOS, however Ni shows the lowest. This is manifested in the values of magnetic moments. The component-projected and the average magnetic moments (in Bohr magnetons/atom) for the three alloy systems are given in Table II. One can

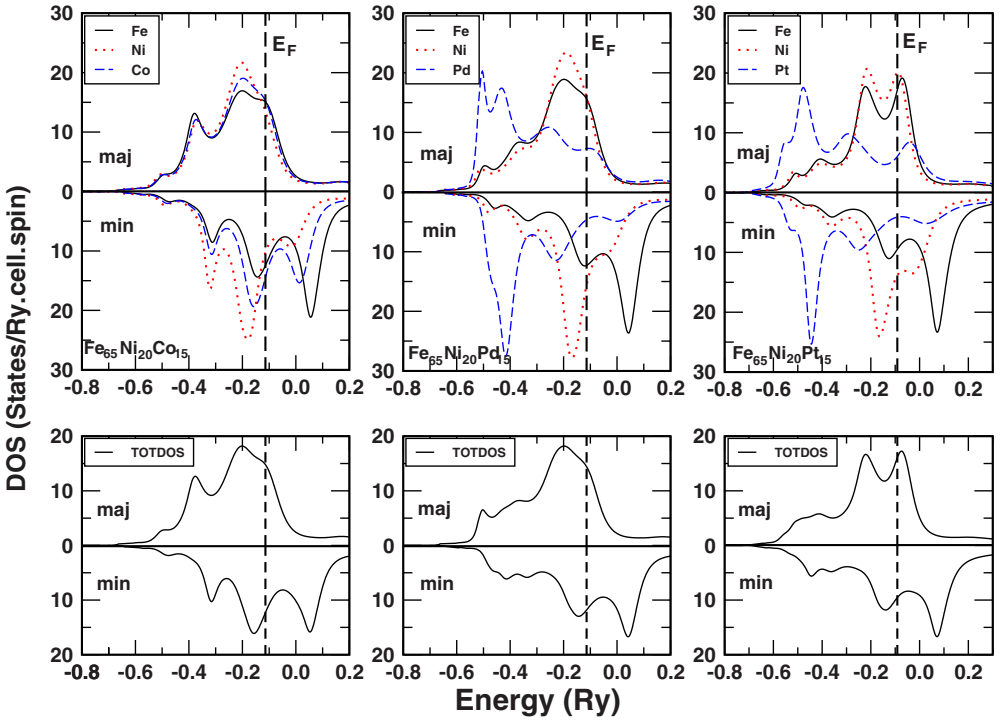

FIG. 8. (Color online) Partial and total density of states for three disordered alloys $Fe_{65}Ni_{20}Co_{15}$ (left), $Fe_{65}Ni_{20}Pd_{15}$ (middle), and $Fe_{65}Ni_{20}Pt_{15}$ (right). The upper row shows the atom-projected DOS for the three alloys (both majority and minority spins). The solid (black), dotted (red), and dashed (blue) lines correspond to the local DOS for Fe, Ni, and X (Co, Pd, and Pt) atoms, respectively. The bottom row however shows the total DOS for the same three alloys. The Fermi levels are indicated by dashed vertical lines.

TABLE II. Component-projected and average magnetic moment (in Bohr magnetons/atom) for $Fe_{65}Ni_{20}X_{15}$ [X=Co,Pd,Pt] alloy systems.

System	m_{Fe}	m_{Ni}	m_X	m_{avg}
$Fe_{65}Ni_{20}Co_{15}$	2.53	0.68	1.41	1.99
$Fe_{65}Ni_{20}Pd_{15}$	2.62	0.69	0.24	1.88
$Fe_{65}Ni_{20}Pt_{15}$	2.51	0.71	0.20	1.80

easily notice that the Fe moment is slightly higher in Pd-substituted alloy while the Ni moments remain almost the same in all the alloys. It is quite interesting to note that Pd and Pt, in spite of being nonmagnetic in the pure state, acquire magnetic moments in the alloy due to the presence of magnetic neighbors Fe and Ni around them. On the other hand Co which is ferromagnetic in the pure state, experiences a diminished magnetism in the alloy. These magnetic properties are in agreement with the results of previous studies on such alloys.[33]

VI. CONCLUSION

The aim of this work was to present a generalized ASR method in the reciprocal-space representation to study the electronic structure of disordered ternary alloys. The formalism allows the calculation of Bloch spectral function at any point in the reciprocal space within the TBLMTO-ASR framework. The efficacy of the formalism was illustrated by examining the electronic structure of the face-centered-cubic based German silver $Cu_{50}Ni_{25}Zn_{25}$ and the magnetic Invar $Fe_{65}Ni_{20}X_{15}$ [X=Co,Pd,Pt] solid solution. The sensitivity of the electronic structure of Cu_2NiZn to local atomic ordering present in the various structural phases is demonstrated carefully. The effects of short-range ordering in this alloy are shown to be quite dramatic. The results for the FeNiX ternary alloys show remarkable similarity with the binary alloys with regard to the general Invar behavior. Our computed magnetic moments follow a general trend as compared to the earlier theoretical findings.

The spectral function provides information on the electronic structure in addition to that contained in the density of states while a knowledge based on the reciprocal-space distribution of the electronic states allows a direct contact to be made with experimental measurements through techniques such as positron annihilation, photoemission, etc. Being encouraged by the correct trend of results for two realistic ternary alloy systems, these techniques will form the basis of further studies into similar alloy systems with varying degrees of complexity and will serve an extensive comparison with other theories and experiments.

ACKNOWLEDGMENTS

One of the authors A.A. would like to acknowledge financial support from the Department of Energy (Grant No. DEFG02-03ER46026) during the time this work was done.

APPENDIX

We present here the effect of the augmented space transfer operators on a general augmented-space "state,"

$$\mathbf{T}_R^{01}\left|\{C_1\}\{C_2\}\right\rangle = \begin{cases} \left|\{C_1+R\}\{C_2\}\right\rangle & \text{if } R\notin\{C_1\}\{C_2\} \\ \left|\{C_1-R\}\{C_2\}\right\rangle & \text{if } R\in\{C_1\} \\ 0 & \text{if } R\in\{C_2\}, \end{cases}$$

$$\mathbf{T}_R^{02}\left|\{C_1\}\{C_2\}\right\rangle = \begin{cases} \left|\{C_1\}\{C_2+R\}\right\rangle & \text{if } R\notin\{C_1\}\{C_2\} \\ 0 & \text{if } R\in\{C_1\} \\ \left|\{C_1\}\{C_2-R\}\right\rangle & \text{if } R\in\{C_2\}, \end{cases}$$

$$\mathbf{T}_R^{12}\left|\{C_1\}\{C_2\}\right\rangle = \begin{cases} 0 & \text{if } R\notin\{C_1\}\{C_2\} \\ \left|\{C_1-R\}\{C_2+R\}\right\rangle & \text{if } R\in\{C_1\} \\ \left|\{C_1+R\}\{C_2-R\}\right\rangle & \text{if } R\in\{C_2\}, \end{cases}$$

$$\mathbf{T}_{RR'}\left|\{C_1\}\{C_2\}\right\rangle = e^{-i\chi}\left|\{C_1\}-\chi,\{C_2\}-\chi\right\rangle,$$

$$\mathbf{T}_{RR'}\left|\{\emptyset\}\{\emptyset\}\right\rangle = e^{-i\chi}\left|\{\emptyset\}\{\emptyset\}\right\rangle.$$

where $\chi=R-R'$.

[1] P. Soven, Phys. Rev. **156**, 809 (1967).
[2] R. J. Elliott, J. A. Krumhansl, and P. L. Leath, Rev. Mod. Phys. **46**, 465 (1974).
[3] H. Ehrenreich and L. Schwartz, *Solid State Physics* (Academic, New York, 1976), Vol. 31, p. 149.
[4] S. Hüfner, G. K. Wertheim, and J. H. Wernick, Phys. Rev. B **8**, 4511 (1973).
[5] A. Zunger, S.-H. Wei, L. G. Ferreira, and J. E. Bernard, Phys. Rev. Lett. **65**, 353 (1990).
[6] M. Jarrell and H. R. Krishnamurthy, Phys. Rev. B **63**, 125102 (2001); D. A. Rowlands, J. B. Staunton, B. L. Györffy, E. Bruno, and B. Ginatempo, *ibid.* **72**, 045101 (2005); D. A. Biava, S. Ghosh, D. D. Johnson, W. A. Shelton, and A. V. Smirnov, *ibid.* **72**, 113105 (2005).
[7] T. Kaplan and M. Mostoller, Phys. Rev. B **9**, 1783 (1974); H. W. Diehl, P. L. Leath, and T. Kaplan, *ibid.* **19**, 5044 (1979); T. Kaplan, P. L. Leath, L. J. Gray, and H. W. Diehl, *ibid.* **21**, 4230 (1980).
[8] S. Ghosh, P. L. Leath, and M. H. Cohen, Phys. Rev. B **66**, 214206 (2002).
[9] T. Saha, I. Dasgupta, and A. Mookerjee, J. Phys.: Condens. Matter **6**, L245 (1994).
[10] A. Mookerjee, J. Phys. C **6**, 1340 (1973).
[11] O. K. Andersen and O. Jepsen, Phys. Rev. Lett. **53**, 2571 (1984).
[12] T. Saha, I. Dasgupta, and A. Mookerjee, Phys. Rev. B **50**, 13267 (1994); T. Saha and A. Mookerjee, J. Phys.: Condens. Matter **8**, 2915 (1996).
[13] A. Alam, S. Ghosh, and A. Mookerjee, Phys. Rev. B **75**, 134202

(2007); A. Alam and A. Mookerjee, *ibid.* **72**, 214207 (2005); J. Phys.: Condens. Matter **18**, 4589 (2006).
[14] I. Dasgupta, T. Saha, and A. Mookerjee, Phys. Rev. B **51**, 3413 (1995); A. Alam, T. Saha-Dasgupta, A. Mookerjee, A. Chakrabarti, and G. P. Das, *ibid.* **75**, 134203 (2007).
[15] K. Tarafder, S. Ghosh, B. Sanyal, O. Eriksson, A. Mookerjee, and A. Chakrabarti, J. Phys.: Condens. Matter **20**, 445201 (2008).
[16] D. A. Rowlands, X. G. Zhang, and A. Gonis, Phys. Rev. B **78**, 115119 (2008).
[17] D. A. Rowlands, A. Ernst, B. L. Györffy, and J. B. Staunton, Phys. Rev. B **73**, 165122 (2006).
[18] A. Mookerjee and P. K. Thakur, Phys. Rev. B **38**, 3798 (1988).
[19] T. Saha and A. Mookerjee, J. Phys.: Condens. Matter **9**, 6607 (1997).
[20] A. Alam and A. Mookerjee, J. Phys.: Condens. Matter **21**, 195503 (2009).
[21] P. Biswas and B. Sanyal, M. Fakhruddin, A. Halder, A. Mookerjee, and M. Ahmed, J. Phys.: Condens. Matter **7**, 8569 (1995).
[22] Order-disorder transitions in Cu_2NiZn have been studied by electrical resistivity measurments [A. De Rooy, G. J. L. Van Der Wegen, P. M. Bronsveld, and J. Th. M. De Hosson, Scr. Metall. **15**, 1362 (1981)]; as well as by transmission electron microscope [G. J. L. Van Der Wegen, A. De Rooy, P. M. Bronsveld, and J. Th. M. De Hosson, *ibid.* **15**, 1359 (1981)]; and neutron diffraction [G. J. L. Van Der Wegen, R. Helmholdt, P. M. Bronsveld, and J. Th. M. De Hosson, Z. Metallkd. **74**, 592 (1983)].
[23] R. Haydock, V. Heine, and M. J. Kelly, J. Phys. C **5**, 2845 (1972).
[24] O. Jepsen, O. K. Andersen, and A. R. Mackintosh, Phys. Rev. B **12**, 3084 (1975).
[25] A. Mookerjee, *Electronic Structure of Alloys, Surfaces and Clusters*, edited by D. D. Sarma and A. Mookerjee (Taylor & Francis, London, 2003).
[26] N. Beer and D. G. Pettifor, in *Electronic Structure of Complex Systems*, edited by P. Phariseau and W. M. Tammerman (Plenum, New York, 1984), p. 769.
[27] R. Haydock, *Lecture Notes in Physics* (Academic Press, New York, 1980), Vol. 35.
[28] A. Mookerjee and R. Prasad, Phys. Rev. B **48**, 17724 (1993).
[29] K. K. Saha, T. Saha-Dasgupta, A. Mookerjee, and I. Dasgupta, J. Phys.: Condens. Matter **16**, 1409 (2004).
[30] K. K. Saha, A. Mookerjee, and O. Jepsen, Phys. Rev. B **71**, 094207 (2005).
[31] U. von Barth and L. Hedin, J. Phys. C **5**, 1629 (1972).
[32] J. Kudrnovský and V. Drchal, Phys. Rev. B **41**, 7515 (1990).
[33] B. Sanyal and S. K. Bose, Phys. Rev. B **62**, 12730 (2000).
[34] A. Alam, T. Saha-Dasgupta, and A. Mookerjee, Phys. Rev. B **81**, 054201 (2010).
[35] D. D. Johnson, A. Alam, and A. V. Smirnov, *MECCA: Multiple-Scattering Electronic-Structure Calculations for Complex Alloys* (University of Illinois, Illinois, 2008); A. Alam and D. D. Johnson, Phys. Rev. B **80**, 125123 (2009).
[36] A. Mookerjee and R. P. Singh, J. Phys. C **18**, 4261 (1985); J. Phys. F: Met. Phys. **18**, 2171 (1988).
[37] J. S. Faulkner, Prog. Mater. Sci. **27**, 1 (1982).
[38] J. D. Althoff, D. D. Johnson, F. J. Pinski, and J. B. Staunton, Phys. Rev. B **53**, 10610 (1996).
[39] J. D. Althoff, D. D. Johnson, and F. J. Pinski, Phys. Rev. Lett. **74**, 138 (1995).